Title

Phosphate Lattice Loss Simulation

Authors

Mohammad Abutayeh, Department of Chemical Engineering, University of South Florida, abutayeh@mail.usf.edu
Scott W. Campbell, Department of Chemical Engineering, University of South Florida, campbell@eng.usf.edu

Citation

M. Abutayeh and S. W. Campbell, Phosphate Lattice Loss Simulation, AIChE–Central Florida Section: International Phosphate Fertilizer & Sulfuric Acid Technology Conference, Clearwater, FL, June 2010

Acknowledgment

The knowledge and guidance provided by Dr. Carlos Busot, Emeritus Professor, Department of Chemical Engineering, University of South Florida, is gratefully acknowledged

Abstract

Phosphoric acid production via the dihydrate process entails inevitable phosphate losses due to gypsum precipitation while extracting phosphoric acid from phosphate rock. Phosphate lattice loss is one type of those losses that occurs due to the incorporation of dicalcium phosphate dihydrate byproduct into the solid gypsum phase in the extracting reactor. A model was developed to simulate the dihydrate process with the aim of quantifying the thermodynamically–controlled phosphate lattice loss. The model assumes equilibrium between liquid and solid phases in the reactor and employs the Edwards–Maurer–Newman–Prausnitz Pitzer–based electrolyte activity coefficient model to express the behavior of a very complexing system of ions and molecules. Temperature–stamped equilibrium data was used to adjust a few parameters via non–linear regression. Model prediction of phosphate lattice loss matched well with experimental values validating the developed model. Decreasing temperature and increasing sulfate levels was found to raise the acidity and the ionic strength of the solution as well as minimize the phosphate lattice loss.

Keywords

Dihydrate process, phosphoric acid, citrate soluble loss, phosphate lattice loss

Introduction

Phosphoric acid is produced from phosphate rock by the dihydrate process in most of the fertilizer plants in Florida. Figure 1 illustrates that process where phosphate rock, rich with tricalcium phosphate, is crushed into small granules then sent to a stirred reactor along with sulfuric acid and water where phosphoric acid is extracted as

$$Ca_3(PO_4)_2 + 3H_2SO_4 + 6H_2O \longrightarrow 2H_3PO_4 + 3CaSO_4 \cdot 2H_2O$$

The products along with the unutilized reactants and byproducts are filtered and then clarified to separate phosphoric acid from the solid gypsum cake. Additional water is used to wash off phosphoric acid from gypsum and to obtain the desired concentration [1].

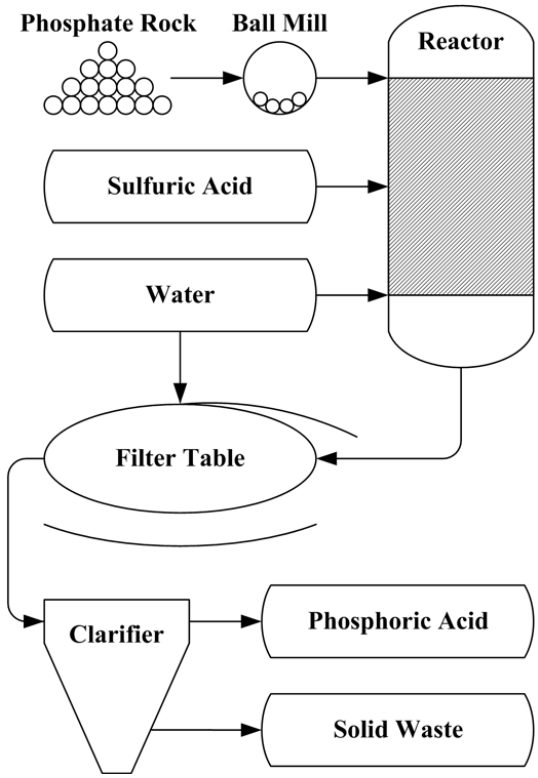

Figure 1. Phosphoric acid production by the dihydrate process

Minimizing the phosphate loss is an essential part in optimizing the dihydrate process. Phosphate loss takes place in different forms and is largely attributed to gypsum crystallization. Gypsum crystals are shown in Figure 2 where the length of the shown bar is 100 Å.

Figure 2. Gypsum crystals

One type of phosphate loss takes place during the filtering of the reaction slurry where some of the phosphoric acid fails to wash away from the solid filter cake. This type of loss can be curtailed by increasing the filter size or by using excess washing water.

A second type of phosphate loss occurs due to poor mixing in the reactor. When phosphate rock encounters a local high concentration of sulfuric acid, gypsum will rapidly precipitate over unreacted rock granules forming crystals with unutilized phosphate inner core. This type of loss can be overcome by improving the mixing mechanism to eliminate the local over–concentrated zones in the reactor.

A third type of phosphate loss arises from the unintended formation of dicalcium phosphate dihydrate, DCPD. Gypsum and DCPD have the same molecular weight and density, share the same monoclinic crystal lattice structure, and their anion groups have matching ionic radius, all of which lead to the formation of a solid solution of both crystals. This lattice loss can be thermodynamically controlled.

The objective of this study is to produce a reliable thermodynamic model that will predict the distribution of phosphates between the liquid and the solid phases in the phosphoric acid reactor of the dihydrate process. In other words, the objective is to build a model that quantifies the lattice loss to study its controlling variables.

Background

Fröchen and Becker [2] experimentally confirmed the existence of a DCPD–Gypsum solid solution. They hypothesized that a number of hydrated phosphate ions replace some sulfate ions in the gypsum lattice due to their similar properties. Janikowski et al. [3] simulated the dihydrate process experimentally at conditions similar to plant operation. Experimental results were reported and the phosphate content of the solid phase was described as a lattice loss.

Griffith [4] and Abutayeh [5] independently attempted to place a thermodynamic bound on the lattice loss of the dihydrate process and compared their predictions to experimental data. Concentration profiles produced by their models accurately depicted the trend of experimental data, but were not quantitatively accurate probably due to the activity coefficient correlations used in their models.

Mathias and Mendez [6] modeled the production of phosphoric acid by the dihydrate process using AspenPlus™. Their model and its parameters were not disclosed due to the commercial nature of their work; however, the results of their simulations were compared to several experimental data yielding very compatible results.

Model

The extracting reactor contains the three distinct phases. The vapor phase can be considered an inert phase due to the low volatility of the reacting species as well as the small solubility of gases in the condensed phases. The liquid phase is mainly water together with phosphoric acid and small amounts of sulfuric acid. The solid phase is mainly gypsum with a little phosphate present as DCPD.

Only major components and reactions need to be considered in a thermodynamic analysis. Trace components and reactions may slightly influence chemical kinetics but not the thermodynamic equilibrium. The phosphate lattice loss model will be developed based upon the following equilibrium reactions

$$H_3PO_4 \longleftrightarrow H^+ + H_2PO_4^-$$
$$H_2PO_4^- \longleftrightarrow H^+ + HPO_4^{2-}$$
$$HSO_4^- \longleftrightarrow H^+ + SO_4^{2-}$$
$$CaHPO_4 \cdot 2H_2O \longleftrightarrow Ca^{2+} + HPO_4^{2-} + 2H_2O$$
$$CaSO_4 \cdot 2H_2O \longleftrightarrow Ca^{2+} + SO_4^{2-} + 2H_2O$$

Very slow chemical reactions, such as the dissolution of H_2O and HPO_4^{2-}, and very fast chemical reactions, such as the dissolution of H_2SO_4, do not disturb equilibrium and thus will not be considered.

Defining total phosphate molality and total sulfate molality

$$TPM = m_{H_3PO_4} + m_{H_2PO_4^-} + m_{HPO_4^{2-}} \quad (1)$$

$$TSM = m_{HSO_4^-} + m_{SO_4^{2-}} \quad (2)$$

Total calcium content of the liquid phase is known as lime solubility and can be expressed as mass percent of CaO equivalence

$$\%CaO = \left(m_{Ca^{2+}} \cdot \Theta_{CaO} \cdot MW_{CaO} \cdot \Phi_{H_2O}\right) \times 100 \quad (3)$$

Total phosphate content of the liquid phase is usually an established parameter and is expressed as mass percent of P_2O_5 equivalence

$$\%P_2O_5 = \left(TPM \cdot \Theta_{P_2O_5} \cdot MW_{P_2O_5} \cdot \Phi_{H_2O}\right) \times 100 \quad (4)$$

Total sulfate content of the liquid phase is a manipulated parameter and is expressed as mass percent of H_2SO_4 equivalence

$$\%H_2SO_4 = \left(TSM \cdot \Theta_{H_2SO_4} \cdot MW_{H_2SO_4} \cdot \Phi_{H_2O}\right) \times 100 \quad (5)$$

Θ_i corresponds to the equivalence moles of species i per mole of its prospective compounds; therefore, Θ_{CaO} is equal to 1, Θ_{P2O5} is equal to ½, and Θ_{H2SO4} is equal to 1. MW_i is the molecular weight of species i and Φ_{H2O} is the mass fraction of water in liquid given by

$$\Phi_{H_2O} = M_{H_2O} / M_{Total} \quad (6)$$

M_i represents the total mass of i per total mass of water in the liquid. This corresponds to a value of unity for M_{H2O} and a value greater than unity for M_{Total}. Conducting a liquid phase total mass balance for all species

$$M_{TPM} = m_{H_3PO_4} \cdot MW_{H_3PO_4} + m_{H_2PO_4^-} \cdot MW_{H_2PO_4^-} + m_{HPO_4^{2-}} \cdot MW_{HPO_4^{2-}} \quad (7)$$

$$M_{TSM} = m_{HSO_4^-} \cdot MW_{HSO_4^-} + m_{SO_4^{2-}} \cdot MW_{SO_4^-} \quad (8)$$

$$M_{Other} = m_{H^+} \cdot MW_{H^+} + m_{Ca^{2+}} \cdot MW_{Ca^{2+}} \quad (9)$$

$$M_{Total} = M_{H_2O} + M_{TPM} + M_{TSM} + M_{Other} \quad (10)$$

A charge balance to satisfy the electro–neutrality condition

$$z_{H_2PO_4^-} m_{H_2PO_4^-} + z_{HPO_4^{2-}} m_{HPO_4^{2-}} + z_{HSO_4^-} m_{HSO_4^-} + z_{SO_4^{2-}} m_{SO_4^{2-}} + z_{H^+} m_{H^+} + z_{Ca^{2+}} m_{Ca^{2+}} = 0 \quad (11)$$

Liquid phase equilibria are included by the dissolution relations of phosphoric acid, phosphate dihydrate, and sulfate hydrate

$$K_{H_3PO_4} = \frac{a_{H_2PO_4^-} \cdot a_{H^+}}{a_{H_3PO_4}} \quad (12)$$

$$K_{H_2PO_4^-} = \frac{a_{HPO_4^{2-}} \cdot a_{H^+}}{a_{H_2PO_4^-}} \quad (13)$$

$$K_{HSO_4^-} = \frac{a_{SO_4^{2-}} \cdot a_{H^+}}{a_{HSO_4^-}} \quad (14)$$

Solid–liquid equilibria are included in the model by the solubility product relations of DCPD and gypsum

$$Ksp_{DCPD} = \frac{a_{HPO_4^{2-}} \cdot a_{Ca^{2+}} \cdot a_{H_2O}{}^2}{a_{DCPD}} \quad (15)$$

$$Ksp_{Gypsum} = \frac{a_{SO_4^{2-}} \cdot a_{Ca^{2+}} \cdot a_{H_2O}{}^2}{a_{Gypsum}} \quad (16)$$

Equilibrium constants as functions of temperature are obtained by integrating van 't Hoff equation assuming a constant heat capacity

$$\ln K_{H_3PO_4} = \ln K^\circ_{H_3PO_4} - \frac{\Delta H^\circ_{H_3PO_4}}{R}\left(\frac{1}{T} - \frac{1}{T^\circ}\right) - \frac{\Delta Cp^\circ_{H_3PO_4}}{R}\left(\ln\frac{T^\circ}{T} - \frac{T^\circ}{T} + 1\right) \quad (17)$$

$$\ln K_{H_2PO_4^-} = \ln K^\circ_{H_2PO_4^-} - \frac{\Delta H^\circ_{H_2PO_4^-}}{R}\left(\frac{1}{T} - \frac{1}{T^\circ}\right) - \frac{\Delta Cp^\circ_{H_2PO_4^-}}{R}\left(\ln\frac{T^\circ}{T} - \frac{T^\circ}{T} + 1\right) \quad (18)$$

$$\ln K_{HSO_4^-} = \ln K^\circ_{HSO_4^-} - \frac{\Delta H^\circ_{HSO_4^-}}{R}\left(\frac{1}{T} - \frac{1}{T^\circ}\right) - \frac{\Delta Cp^\circ_{HSO_4^-}}{R}\left(\ln\frac{T^\circ}{T} - \frac{T^\circ}{T} + 1\right) \quad (19)$$

$$\ln K_{DCPD} = \ln K^\circ_{DCPD} - \frac{\Delta H^\circ_{DCPD}}{R}\left(\frac{1}{T} - \frac{1}{T^\circ}\right) - \frac{\Delta Cp^\circ_{DCPD}}{R}\left(\ln\frac{T^\circ}{T} - \frac{T^\circ}{T} + 1\right) \quad (20)$$

$$\ln K_{Gypsum} = \ln K^\circ_{Gypsum} - \frac{\Delta H^\circ_{Gypsum}}{R}\left(\frac{1}{T} - \frac{1}{T^\circ}\right) - \frac{\Delta Cp^\circ_{Gypsum}}{R}\left(\ln\frac{T^\circ}{T} - \frac{T^\circ}{T} + 1\right) \quad (21)$$

Reference state thermodynamic properties of the reacting species are widely available in literature and can be used to evaluate the reference state reaction thermodynamic properties above as follows: $\ln(K^\circ) = -\Delta G^\circ / (R \cdot T^\circ)$, $\Delta G^\circ = \Sigma(\nu_i \cdot G^\circ_i)$, $\Delta H^\circ = \Sigma(\nu_i \cdot H^\circ_i)$, $\Delta Cp^\circ = \Sigma(\nu_i \cdot Cp^\circ_i)$.

An alternative approach for expressing the equilibrium constants was used in this model. Experimental data of equilibrium constants [7] and solubility products [8–10] of model reactions were found at various temperatures. Least squares regression was used to fit data points to the above equilibrium constant equations by manipulating the values of ΔCp° and ΔH°. This approach compensates for the temperature–independent heat capacity assumption used to develop the above equilibrium constant equations resulting in better estimates of the equilibrium constants. Table 1 summarizes the least squares regression results. It is important to note that the adjusted values of $\Delta Cp°$ and $\Delta H°$ given in Table 1 no longer represent the heat capacity and enthalpy of dissolution of model reactions, but rather the adjusted parameters used in expressing the equilibrium constants of model reactions as functions of temperature.

Table 1. Experimental and regressed values of equilibrium reactions

Equilibrium Reaction	*Experimental K°*	*Adjusted ΔCp°*	*Adjusted ΔH°*
$H_3PO_4 \longleftrightarrow H^+ + H_2PO_4^-$	7.112E-3 7	-155	-7663
$H_2PO_4^- \longleftrightarrow H^+ + HPO_4^{2-}$	6.340E-8 7	-249	4034
$HSO_4^- \longleftrightarrow H^+ + SO_4^{2-}$	1.030E-2 7	-310	-16928
$CaSO_4 \cdot 2H_2O \longleftrightarrow Ca^{2+} + SO_4^{2-} + 2H_2O$	4.220E-5 8	-494	4338
$CaHPO_4 \cdot 2H_2O \longleftrightarrow Ca^{2+} + HPO_4^{2-} + 2H_2O$	2.513E-7 9	-879	-3050

Ionic strength is used in measuring deviations from ideality in ionic solutions. The ionic strength of the solution can be written as

$$I = \frac{m_{H_2PO_4^-} z^2_{H_2PO_4^-} + m_{HPO_4^{2-}} z^2_{HPO_4^{2-}} + m_{HSO_4^-} z^2_{HSO_4^-} + m_{SO_4^{2-}} z^2_{SO_4^{2-}} + m_{H^+} z^2_{H^+} + m_{Ca^{2+}} z^2_{Ca^{2+}}}{2} \quad (22)$$

The hydrogen ion activity in solution is a very important concept and the magnitude of this activity is measured by the pH

$$pH = -log_{10}\left(a_{H^+} \cdot \rho_{H_2O}\right) \quad (23)$$

Note that the mass density of water was used to convert the activity concentration scale from molality to molarity as required by the pH definition. In other words, pH is the negative 10–base logarithm of hydrogen ion activity given on a molarity scale. The mass density of water can be calculated as a function of temperature by [11]

$$\rho_{H_2O} = 1 - \frac{(T+16)\cdot(T-277)^2}{(508929)\cdot(T-205)} \quad (24)$$

The electrostatic forces between different ions in a solution depend on the polarity of the solvent. The dielectric constant of a solvent is a measure of its polarity and is widely used in modeling molecular interactions. The Dielectric constant of water is calculated by [12]

$$D' = 305.7 \cdot exp\left(-exp(-12.741 + 0.01875 \cdot T) - \frac{T}{219}\right) \quad (25)$$

Phosphate lattice loss is expressed as percent of P_2O_5 equivalence

$$\%P_2O_5^{(S)} = \left(\omega_{DCPD} \cdot \left(\frac{1}{MW_{DCPD}}\right) \cdot \Psi_{P_2O_5} \cdot MW_{P_2O_5}\right) \times 100 \quad (26)$$

Ψ_{P2O5} corresponds to the equivalence moles of P_2O_5 per mole of DCPD; therefore, Ψ_{P2O5} is equal to ½. ω_{DCPD} is the mass fraction of DCPD in the solid solution given by

$$\omega_{DCPD} = \frac{x_{DCPD} \cdot MW_{DCPD}}{x_{Gypsum} \cdot MW_{Gypsum} + x_{DCPD} \cdot MW_{DCPD}} \quad (27)$$

Neglecting the presence of impurities and assuming that the solid phase consists of only gypsum and DCPD

$$x_{DCPD} + x_{Gypsum} = 1 \quad (28)$$

The activity coefficients of the reacting species are used to modify their concentrations to account for deviation from ideality. Activity is defined as: $a_i = \gamma_i \cdot (m_i / m^\circ)$, where m° is the reference state unit molality which is normally omitted with the understanding that both activity and activity coefficient are dimensionless. Relating activity to molality using activity coefficient for each reacting specie [13]

$$a_{H_3PO_4} = \gamma_{H_3PO_4} \cdot m_{H_3PO_4} \tag{29}$$

$$a_{H_2PO_4^-} = \gamma_{H_2PO_4^-} \cdot m_{H_2PO_4^-} \tag{30}$$

$$a_{HPO_4^{2-}} = \gamma_{HPO_4^{2-}} \cdot m_{HPO_4^{2-}} \tag{31}$$

$$a_{HSO_4^-} = \gamma_{HSO_4^-} \cdot m_{HSO_4^-} \tag{32}$$

$$a_{SO_4^{2-}} = \gamma_{SO_4^{2-}} \cdot m_{SO_4^{2-}} \tag{33}$$

$$a_{H^+} = \gamma_{H^+} \cdot m_{H^+} \tag{34}$$

$$a_{Ca^{2+}} = \gamma_{Ca^{2+}} \cdot m_{Ca^{2+}} \tag{35}$$

$$a_{DCPD} = \gamma_{DCPD} \cdot x_{DCPD} \tag{36}$$

$$a_{Gypsum} = \gamma_{Gypsum} \cdot x_{Gypsum} \tag{37}$$

Activity Coefficients

The Debye–Hückel theory [14] introduced in 1923 revolutionized the way electrolytes are modeled by accounting for the electrostatic forces present between ions in solutions. Several electrolyte models have been developed based on the Debye–Hückel theory with most including adjustable parameters to improve their predictions.

Griffith [4] used Bromley correlation [15] while Abutayeh [5] used Robinson–Guggenheim–Bates correlation [7] to express the activity coefficients of ions in their attempts to model phosphate lattice loss. In addition, they both used experimental vapor pressure data [16] to predict the activity of uncharged species. The phosphate lattice loss predicted by both was about half that of reported data. Abutayeh later improved his model by replacing the activity correlations of the uncharged species with correlations reported by Ziat et al. [17].

Mathias and Mendez [6] used the Electrolyte–NRTL model [18] to calculate the activity coefficients of all species to simulate the dihydrate process. The Electrolyte–NRTL model can express the activity coefficients of both charged and uncharged species, but it includes many interaction parameters that must be experimentally determined. Messnaoui and Bounahmidi [19] modeled a similar system using the Electrolyte–NRTL model; however, many interaction parameters were either neglected or arbitrarily fixed.

The current model is very non–linear due to very different values of equilibrium constants; therefore, a potent activity coefficient model is needed. The Edwards–Maurer–Newman–Prausnitz Pitzer–based model [20] is a comprehensive model that can express the activity of charged and uncharged species in a multi–component solution. It is incorporated into the current model because of its objective and straightforward approach to obtaining the interaction parameters.

Writing the activity coefficients of all ions and molecules is lengthy but straightforward; thus, abbreviated activity coefficient relations will be stated. The activity coefficients of all ions and molecules in solution are given by

$$ln\gamma_i = z_i^2 \cdot f + 2 \cdot X_i + z_i^2 \cdot Y \tag{38}$$

The solid phase can be safely assumed ideal since it mainly consists of slightly soluble gypsum. DCPD is present in very small amounts in the solid phase with physical properties very similar to those of gypsum, furthering the validity of ideal solid solution assumption. The activity coefficients in the solid phase are therefore written as

$$\gamma_{Gypsum} = \gamma_{DCPD} = 1 \tag{39}$$

The Edwards–Maurer–Newman–Prausnitz Pitzer–based model also offers an expression for water activity

$$ln\, a_{H_2O} = MW_{H_2O} \cdot \left[\frac{2 \cdot A \cdot I^{3/2}}{1 + 1.2 \cdot \sqrt{I}} - Z - \sum_{i \neq H_2O} m_i \right] \tag{40}$$

The included electrostatic functions are defined by

$$A = \frac{1}{3} \cdot \sqrt{2000 \cdot \pi \cdot N_A \cdot \rho_{H_2O}} \cdot \left[\frac{e^2}{4 \cdot \pi \cdot \varepsilon_0 \cdot D' \cdot k \cdot T} \right]^{3/2} \tag{41}$$

$$f = -A \cdot \left[\frac{\sqrt{I}}{1 + 1.2 \cdot \sqrt{I}} + \frac{2}{1.2} \cdot ln\left(1 + 1.2 \cdot \sqrt{I}\right) \right] \tag{42}$$

$$Y = \sum_{i \neq H_2O} Y_i \tag{43}$$

$$Z = \sum_{i \neq H_2O} Z_i \tag{44}$$

The colligative properties of the activity coefficient model are

$$X_i = \sum_{j \neq H_2O} B_{i-j} \cdot m_j \tag{45}$$

$$Y_i = \sum_{j \neq H_2O} C_{i-j} \cdot m_i \cdot m_j \tag{46}$$

$$Z_i = \sum_{j \neq H_2O} D_{i-j} \cdot m_i \cdot m_j \tag{47}$$

The interaction terms of the activity coefficient model are given by

$$B_{i-j} = \beta^0_{i-j} + \frac{\beta^1_{i-j}}{2 \cdot I} \cdot \left[1 - \left(1 + 2 \cdot \sqrt{I}\right) \cdot exp\left(-2 \cdot \sqrt{I}\right)\right] \quad (48)$$

$$C_{i-j} = \frac{\beta^1_{i-j}}{4 \cdot I^2} \cdot \left[-1 + \left(1 + 2 \cdot \sqrt{I} + 2 \cdot I\right) \cdot exp\left(-2 \cdot \sqrt{I}\right)\right] \quad (49)$$

$$D_{i-j} = \beta^0_{i-j} + \beta^1_{i-j} \cdot exp\left(-2 \cdot \sqrt{I}\right) \quad (50)$$

The reference state unit molality, m°, was dropped from the above interaction terms. Edwards et al. [20] proposed a simple approach to estimate the interaction parameters in a multi–component solution. Their approach can be summarized as follows:

- If i and j are ions of like charge, $\beta^0_{i-j} = \beta^1_{i-j} = 0$
- If i or j is a molecular species, $\beta^1_{i-j} = 0$
- If i and j are molecular species, $\beta^0_{i-j} = ½ \cdot [\ \beta^0_{i-i} + \beta^0_{j-j}\ ]$
- Molecular self–interaction parameter depends on temperature like so: $\beta^0_{i-i} = E + F / T$
- The remaining ion–ion and ion–molecule interaction parameters are estimated using Bromley's theory of the additivity of single ion interactions [15] given by: $\beta^0_{i-j} = \beta^0_i + \beta^0_j$ and $\beta^1_{i-j} = \beta^1_i + \beta^1_j$

Single interaction parameters are obtained by applying Bromley's additivity theory to binary interaction parameters given by Pitzer and Mayorga [21] at 25 °C for strong electrolytes. β^0_{Na} and β^1_{Na} are arbitrarily set to zero to accomplish this separation.

The above approach was employed to evaluate the required interaction parameters. Table 2 lists the Pitzer's binary interaction parameters [22]–[23] that were used to obtain the single ion interactions listed in Table 3 that were used in the current model. The Edwards–Maurer–Newman–Prausnitz Pitzer–based model is considered viable for aqueous solutions with ionic strengths up to 6 mol/Kg H_2O and for temperatures ranging from 0 to 170 °C.

Lime solubility figures for a dihydrate process at various conditions reported by Mathias and Mendez [6] were used to estimate the molecular self–interaction parameter, $\beta^0_{H3PO4–H3PO4}$. Their reported lime solubility was obtained by a theoretically–based correlation for solutions with sulfate levels varying from 0–5 % at 25 °C and 75 °C with 25 % and 30 % phosphate content. Estimation of $\beta^0_{H3PO4–H3PO4}$ was accomplished by running the model at conditions analogues to those of Mathias and Mendez and matching the lime solubility to their results by adjusting the value of $\beta^0_{H3PO4–H3PO4}$. Least squares regression was then used to fit the obtained $\beta^0_{H3PO4–H3PO4}$ values to the molecular self–interaction parameter function recommended by Edwards et al. [20] obtaining the following relation:

$$\beta^0_{H_3PO_4-H_3PO_4} = 0.3609 + \frac{73.1537}{T} \quad (51)$$

Table 2. Pitzer's interaction parameters

Species	β^0	β^1
$NaCl$	0.0765	0.2664
HCl	0.1775	0.2945
NaH_2PO_4	-0.0533	0.0396
Na_2HPO_4	-0.0583	1.4655
Na_2SO_4	0.0196	1.1130

Table 3. Single interaction parameters

Species	β^0	β^1
H_3PO_4	0.0477	0.0677
$H_2PO_4^-$	-0.053	0.0396
HPO_4^{2-}	-0.058	1.4655
HSO_4^-	0.0257	0.838
SO_4^{2-}	0.0196	1.113
H^+	0.101	0.0281
Ca^{2+}	0.2394	1.3476

Results

A computer code featuring the above equations was developed using TK Solver™. Program execution is simultaneous due to the interdependence of model equations. The code requires providing initial guesses for Φ_{H2O}, m_{H3PO4}, m_{H2PO4-}, m_{HSO4-}, m_{Ca2+}, x_{Gypsum}. Convergence was difficult, but attainable, at times due to rapidly changing system variables at some conditions as will be evident later in the ensuing figures.

Temperature effect on system phase equilibria can be illustrated by Figure 3 through Figure 7 where the equilibrium constants of model reactions were evaluated using the adjusted parameters obtained by regression then plotted versus temperature along with the experimental data. The equilibrium constant relations given above with their adjusted parameters produced excellent depictions of phase equilibria when compared to experimental data.

The model was validated by comparing its phosphate lattice loss prediction to experimental data reported by Janikowski et al. [3] for Moroccan phosphate rock. The trend produced by the model matched well with the reported data as shown by Figure 8. The mean absolute error of all twelve data points was 0.032 while the standard deviation of the calculated values was 0.078.

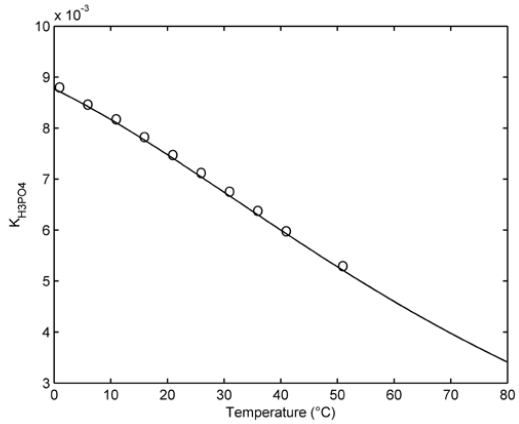

Figure 3. H_3PO_4 equilibrium constant versus temperature

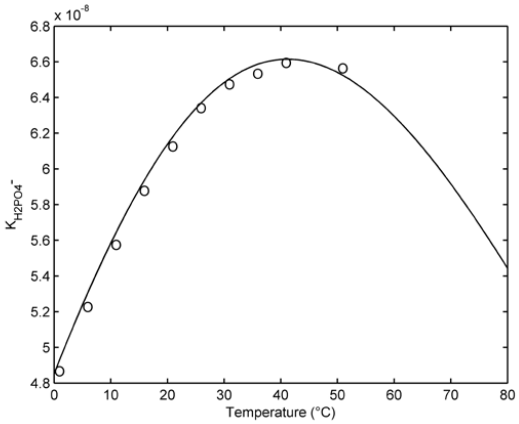

Figure 4. $H_2PO_4^-$ equilibrium constant versus temperature

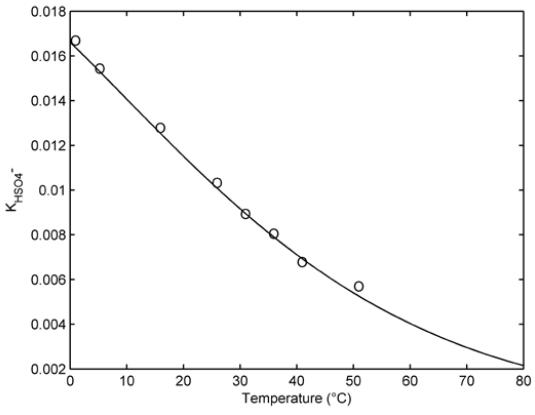

Figure 5. HSO_4^- equilibrium constant versus temperature

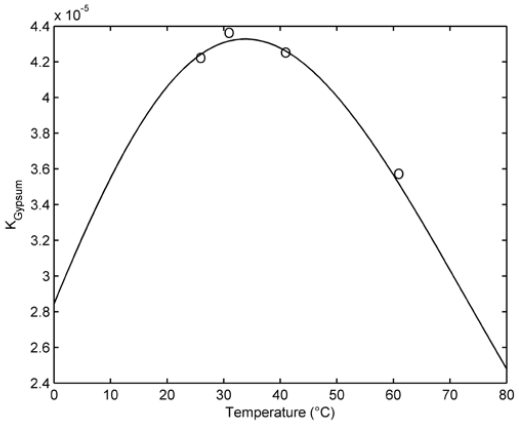

Figure 6. Gypsum equilibrium constant versus temperature

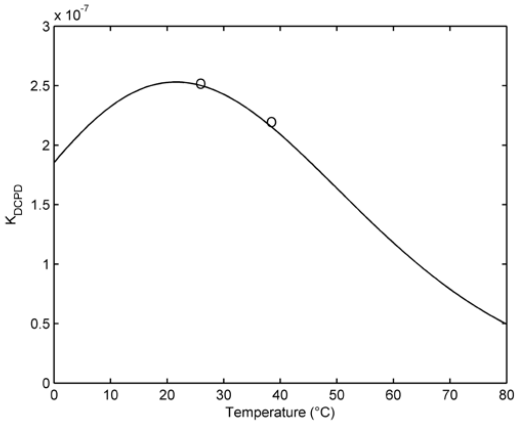

Figure 7. DCPD equilibrium constant versus temperature

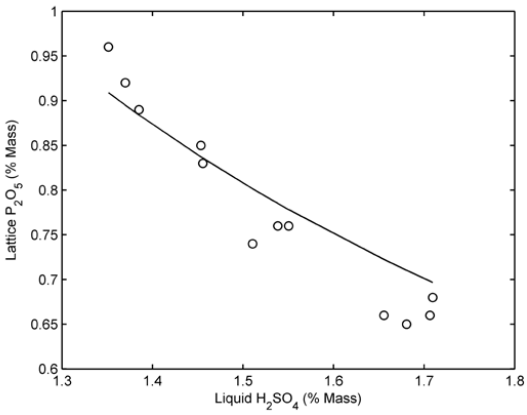

Figure 8. Lattice loss versus sulfates at 79 °C and 31 % phosphates

Sulfate content effect on system variables can be illustrated by Figure 9 through Figure 12 that show model output at 80 °C, 30 % phosphates, and different sulfate levels. For the most part, ionic strength increased while solution pH decreased with increasing sulfate levels due to the increased electrostatic interactions among ions and the increased concentration of the hydrogen ion brought by the enhanced degree of ionization that comes with elevated sulfate content. Increasing sulfate levels shifts the system equilibrium towards less gypsum dissolution marked by decreased lime solubility and decreased phosphate lattice loss.

Temperature plus solution sulfates and phosphates are the main controlling variables of the phosphate lattice loss. Temperature and solution phosphates are essentially set by the operational constraints of the commercial dihydrate process; however, solution sulfates can be manipulated and controlled and seem to have a substantial effect on the phosphate lattice loss as mentioned earlier [3].

System variables depicted above in Figure 9 through Figure 12 were numerically differentiated with respect to solution sulfate levels producing Figure 13 through Figure 16. This straightforward mathematical procedure will help reveal the extent of the influence solution sulfate levels have on system variables. Figure 13 through Figure 16 clearly show that the rate of change of system variables severely decrease as sulfate levels reach 1 % after which they begin to level out. This important observation indicates a rapid initial gypsum precipitation that gradually stabilizes as sulfate levels start to increase which explains the initial sharp drop in ionic strength and pH shown in Figure 9 and Figure 10.

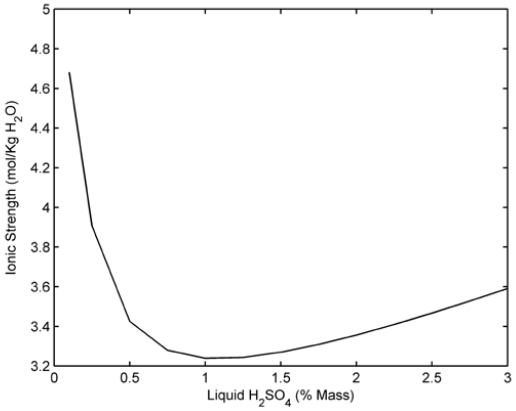

Figure 9. IS versus sulfates at 80 °C and 30 % phosphates

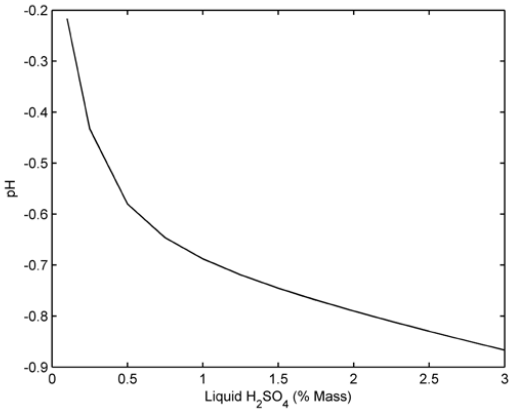

Figure 10. pH versus sulfates at 80 °C and 30 % phosphates

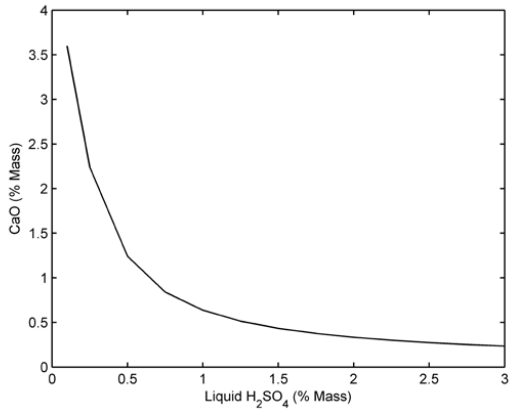

Figure 11. CaO versus sulfates at 80 °C and 30 % phosphates

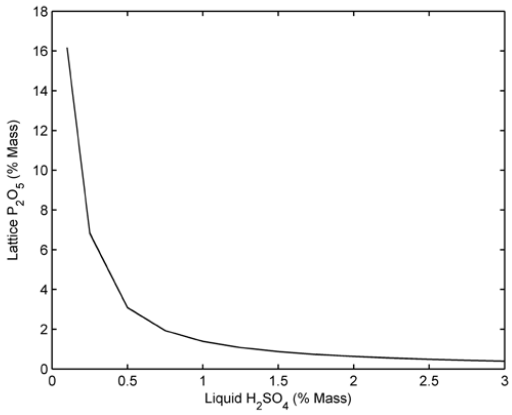

Figure 12. LL versus sulfates at 80 °C and 30 % phosphates

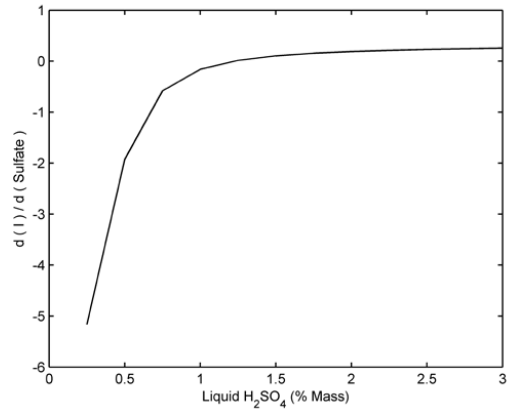

Figure 13. IS ROC versus sulfates at 80 °C and 30 % phosphates

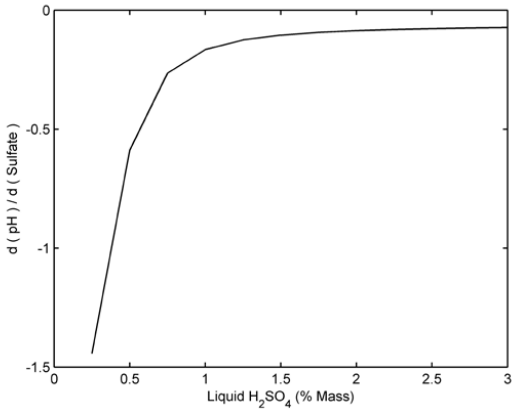

Figure 14. pH ROC versus sulfates at 80 °C and 30 % phosphates

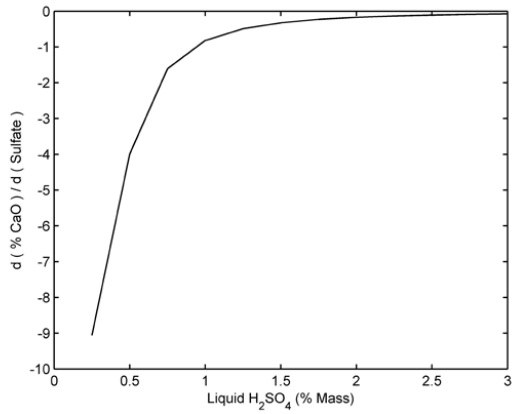

Figure 15. CaO ROC versus sulfates at 80 °C and 30 % phosphates

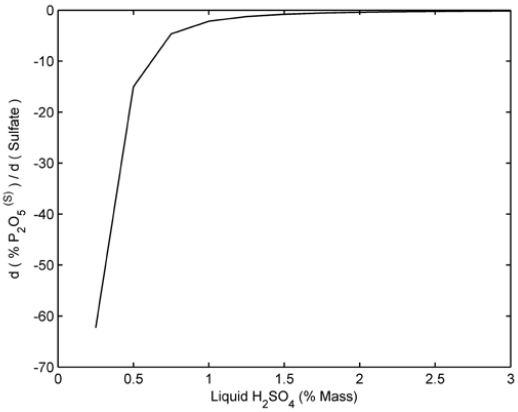

Figure 16. LL ROC versus sulfates at 80 °C and 30 % phosphates

Temperature effect on system variables can be illustrated by Figure 17 through Figure 20 that show model output at 1.5 % sulfates, 30 % phosphates, and different operating temperatures. Ionic strength decreased while solution pH increased with increasing operating temperatures due to the decreased electrostatic interactions among ions and the decreased concentration of the hydrogen ion brought by the reduced degree of ionization that comes with higher temperatures. Increasing operating temperatures shifts the system equilibrium towards more gypsum dissolution marked by increased lime solubility and increased phosphate lattice loss. Conversely, decreasing operating temperatures desirably brings about softer solution and decreased phosphate lattice loss.

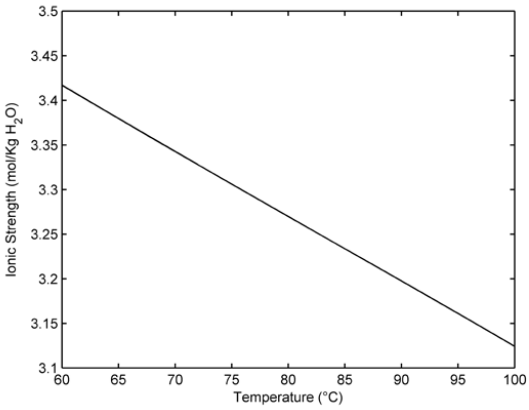

Figure 17. IS vs temperature at 1.5 % sulfates and 30 % phosphates

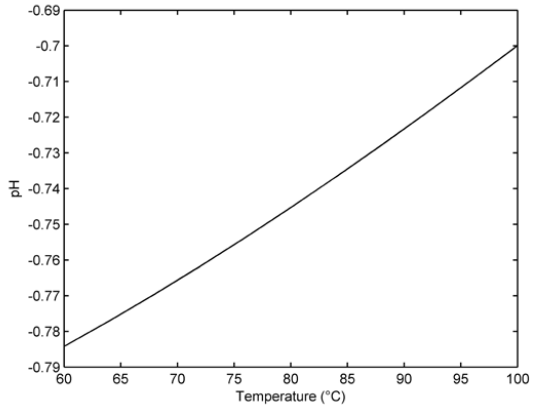

Figure 18. pH vs temperature at 1.5 % sulfates and 30 % phosphates

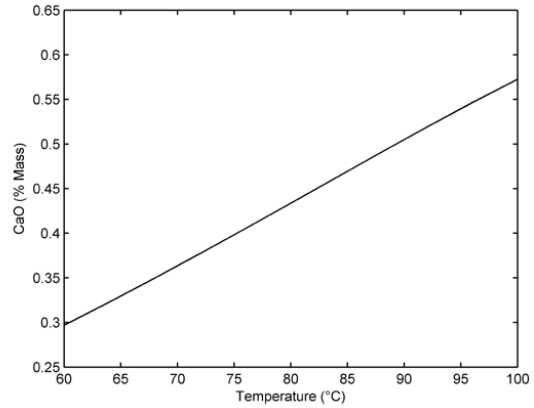

Figure 19. CaO vs temperature at 1.5 % sulfates & 30 % phosphates

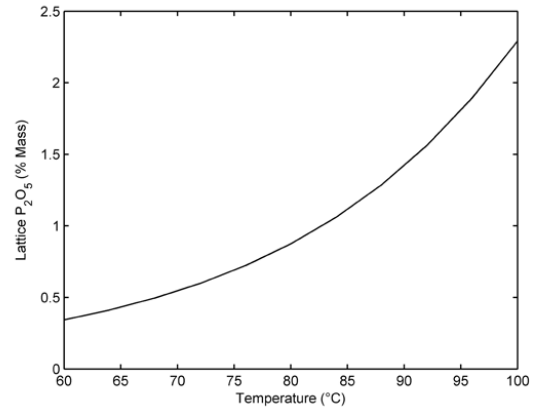

Figure 20. LL vs temperature at 1.5 % sulfates and 30 % phosphates

Phosphate content effect on system variables is given by Figure 21 through Figure 24 that show model output at 80 °C, 1.5 % sulfates, and different phosphate levels. Ionic strength increased and solution pH decreased with increasing phosphate levels due to the increased electrostatic interactions among ions and increased concentration of hydrogen ion brought by enhanced degree of ionization that comes with elevated phosphate content. Increasing phosphate levels up to 28 % shifts system equilibrium to more gypsum dissolution marked by increased lime solubility and phosphate lattice loss; however, increasing phosphate levels beyond 28 % shifts system equilibrium to less gypsum dissolution marked by decreased lime solubility and decreased phosphate lattice loss. Messnaoui and Bounahmidi [19] reported that gypsum dissolution in aqueous phosphoric acid at various temperatures reaches a maximum at about 22 % phosphate concentration based on experimental and calculated results. This observation supports the predictions of the current model.

Conclusion

Phosphoric acid manufacturing by the dihydrate process involves inevitable phosphate losses due to the formation of gypsum crystals. One type of these losses is triggered by the crystallization of DCPD that has the same lattice structure as that of gypsum. As a result, gypsum and DCPD form a solid solution with a thermodynamically controlled composition. Increasing liquid phase content of sulfates or decreasing temperature was found to raise the acidity of the solution and reduce the phosphate lattice loss of dihydrate process.

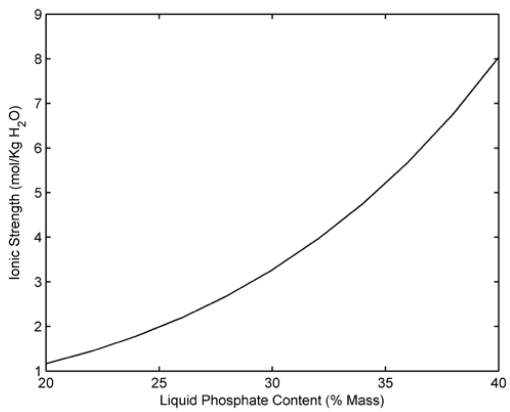

Figure 21. IS versus phosphate levels at 80 °C and 1.5 % sulfates

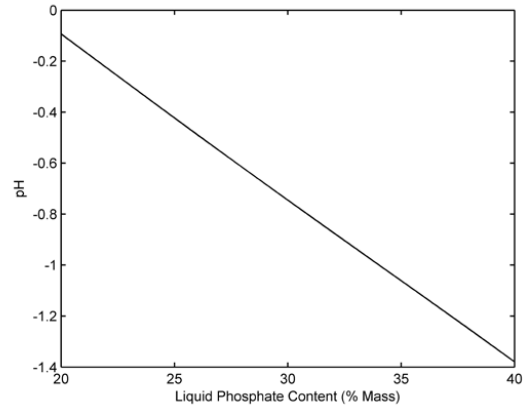

Figure 22. pH versus phosphate levels at 80 °C and 1.5 % sulfates

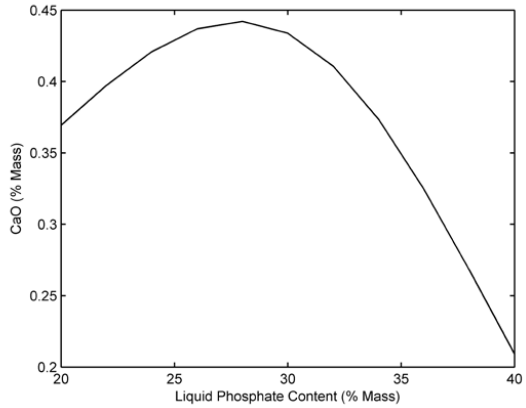

Figure 23. CaO versus phosphate levels at 80 °C and 1.5 % sulfates

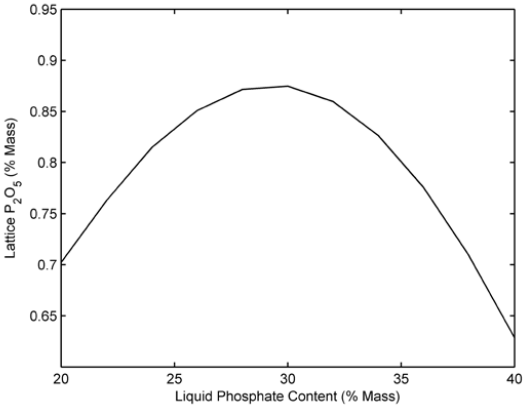

Figure 24. LL versus phosphate levels at 80 °C and 1.5 % sulfates

Recommendations

The current model only considers major components and major reactions in its thermodynamic analysis while other possible impurities are assumed to be too small to influence the system equilibrium. Impurities can substantially shape the thermodynamic equilibrium if present in large quantities; hence, realistic characterization of phosphate rock is crucial to accurate modeling. Possible impurities include fluoride, aluminum, iron, magnesium, sodium, silicate, carbonate, and others.

Temperature–dependent equilibrium constants can be generated by including reliable empirical heat capacity relations in van ‘t Hoff equation before integrating it. This approach is more coherent than the approach of the current model but could inhibit its convergence due to the added mathematical complexity. If the approach of the current model is preferred, finding more equilibrium data at a wider temperature range for all reactions, particularly for the solubility product relations of DCPD and gypsum, is crucial to performing more rigorous regressions to better estimate adjusted parameters.

The extracting reactor of the dihydrate process includes a very complexing system comprising strong and weak electrolytes as well as neutral molecules. Modeling the activity coefficients of this complexing system is very challenging due to the large number of interactions present between all of the different ions and molecules. The present model uses the Edwards–Maurer–Newman–Prausnitz Pitzer–based model for its applicability to both ions and molecules and for its objectivity in obtaining the interaction parameters. The Chen model [24] is widely used for complexing systems but it includes many interaction parameters that must be experimentally determined. Reliable data from the dihydrate process is very scarce but essential in accurately estimating the interaction parameters regardless of which activity coefficient model is used.

Abbreviation

DCPD	Dicalcium phosphate dihydrate
IS	Ionic strength
LL	Lattice loss
ROC	Rate of change
TPM	Total phosphate molality
TSM	Total sulfate molality

Notation

%CaO	Percent CaO equivalence by mass in liquid [Kg CaO/Kg Liquid]
$\%H_2SO_4$	Percent H_2SO_4 equivalence by mass in liquid [Kg H_2SO_4/Kg Liquid]
$\%P_2O_5$	Percent P_2O_5 equivalence by mass in liquid [Kg P_2O_5/Kg Liquid]
$\%P_2O_5^{(S)}$	Percent P_2O_5 equivalence by mass in solid [Kg P_2O_5/Kg Solid]
Θ	Equivalence moles per mole of prospective compound in liquid
Ψ	Equivalence moles per mole of prospective compound in solid
ρ	Mass density [Kg /L]
Φ	Mass fraction in liquid
ω	Mass fraction in solid
γ	Molality based activity coefficient
ΔCp	Molar specific heat of dissolution or solubility [J/(mol·K)]
ΔG	Molar Gibbs free energy of dissolution or solubility [J/mol]
ΔH	Molar enthalpy of dissolution or solubility [J/mol]
β^0	Interaction parameter [Kg H_2O/mol]
β^1	Interaction parameter
ε_0	Permittivity of free space = 8.854E-12 [$C^2/(N\cdot m^2)$]
a	Molality based activity
A	Debye–Hückel constant for osmotic coefficients [(Kg H_2O/mol)½]
B	Interaction term [Kg H_2O/mol]
C	Interaction term [(Kg H_2O/mol)2]
D	Interaction term [Kg H_2O/mol]
D'	Dielectric constant of water
e	Electron charge = 1.602E-19 [C]
f	Pitzer's electrostatic function
I	Ionic strength [mol/Kg H_2O]
k	Boltzmann constant = 1.381E-23 [J/K]
K	Dissolution equilibrium constant
Ksp	Solubility product
m	Molality [mol/Kg H_2O]
M	Mass per mass of water [Kg/Kg H_2O]
MW	Molecular weight [Kg/mol]
NA	Avogadro's number = 6.022137E+23 [1/mol]
pH	pH of liquid
R	Ideal gas constant = 8.314 [J/(mol·K)]
T	Temperature [K]
TPM	Total phosphate molality [mol/Kg H_2O]
TSM	Total sulfate molality [mol/Kg H_2O]
x	Mole fraction in solid
X	Interactions summation
Y	Interactions summation
z	Ionic charge
Z	Interactions summation [mol/Kg H_2O]

References

1. Van Der Sluis, S.; Meszaros, Y.; Wesselingh, J. A.; Van Rosmalen, G. M. A Clean Technology Phosphoric Acid Process. The Fertiliser Society: London, UK, 1986.
2. Fröchen, J.; Becker, P. Crystallization and Co–crystallization in the Manufacture of Wet–Process Phosphoric Acid. Proceedings of the International Superphosphate Manufacturers Association Technical Conference, Stockholm, Sweden 1959, No. LE/59/59.
3. Janikowski, S. M.; Robinson N.; Sheldrick W. F. Insoluble Phosphate Losses in Phosphoric Acid Manufacture by the Wet Process. Proceedings of the Fertilizer Society, London, UK 1961, No. 81.
4. Griffith, D. J. Jr.; Thermodynamic Bounds on Composition of Calcium Sulfate–Calcium Phosphate Solid Solutions in Equilibrium with Phosphoric Acid Solutions, Master Thesis; University of South Florida: Tampa, Florida, 1985.
5. Abutayeh, M.; Thermodynamic Model and the Controlling Variables of Phosphate Lattice Loss, Master Thesis; University of South Florida: Tampa, Florida, 1999.
6. Mathias, P. M.; Mendez, M. Simulation of Phosphoric Acid Production by the Dihydrate Process. Proceedings of the Twenty Second Clearwater Convention on Phosphate Fertilizer and Sulfuric Acid Technology, Clearwater, FL 1998, No. 98.1.4.
7. Dean, J. A. Lange's Handbook of Chemistry, Fourteenth Edition; McGraw–Hill: New York, NY, 1992.
8. Marshall, W. L.; Slusher, R.; Jones, E. V. Aqueous Systems at High Temperature XIV: Solubility and Thermodynamic Relationships for $CaSO_4$ in NaCl–H_2O Solutions from 40° to 200°C, 0 to 4 Molal NaCl. Journal of Chemical and Engineering Data 1964, 9, pp 187–191.
9. Patel, P. R.; Gregory, T. M.; Brown, W. E. Solubility of $CaHPO_4{\cdot}2H_2O$ in the Quaternary System $Ca(OH)_2$–H_3PO_4–NaCl–H_2O at 25 °C. Journal of Research – National Bureau of Standards 1974, 78A(6), pp 675–681.
10. Moreno, E. C.; Gregory, T. M. Solubility of $CaHPO_4{\cdot}2H_2O$ and Formation of Ion Pairs in the System $Ca(OH)_2$–H_3PO_4–H_2O at 37.5 °C. Journal of Research – National Bureau of Standards 1966, 70A(6), pp 545–552.

11. McCutcheon, S. C.; Martin, J. L.; Barnwell, T. O. Jr.; Maidment, D. R., editor. Handbook of Hydrology; McGraw–Hill: New York, NY, 1993.
12. Pottel, R. Dielectric Properties. In Water: A comprehensive Treatise; Franks F., editor; Plenum Press: New York, NY, 1973; Third Volume.
13. Zemaitis, J. F. Jr.; Clark, D. M.; Rafal, M.; Scrivner, N. C. Handbook of Aqueous Electrolyte Thermodynamics. American Institute of Chemical Engineers: New York, NY, 1986.
14. Debye, P.; Hückel, E. The Theory of Electrolytes. Physikalische Zeitschrift 1923, 24, pp 185–206.
15. Bromley, L. A. Thermodynamic Properties of Strong Electrolytes in Aqueous Solutions. Journal of the American Institute of Chemical Engineers 1973, 19(2), pp 313–320.
16. Elmore, K. L.; Mason, C. M.; Christensen, J. H. Activity of Orthophosphoric Acid in Aqueous Solution at 25° from Vapor Pressure Measurements. Journal of the American Chemical Society 1946, 68 (12), pp 2528–2532.
17. Ziat, K.; Mesnaoui, B.; Bounahmidi, T.; Boussen, R.; La Guardia, M.; and Garrigues, S. Modelling of the Ternary System H_3PO_4/H_2O/TBP. Journal of Fluid Phase Equilibria 2002, 201 (2), pp 259–267.
18. Chen, C. C.; Britt, H. I.; Boston, J. F.; Evans, L. B. Local Composition Model for Excess Gibbs Energy of Electrolyte Systems. Journal of the American Institute of Chemical Engineers 1982, 28, pp 588–596.
19. Messnaoui, B.; Bounahmidi, T. On the Modeling of Calcium Sulfate Solubility in Aqueous Solutions. Journal of Fluid Phase Equilibria 2006, 244 (2), pp 117–127.
20. Edwards, T. J.; Maurer, G.; Newman, J.; Prausnitz, J. M. Vapor–Liquid Equilibria in Multicomponent Aqueous Solutions of Volatile Weak Electrolytes. Journal of the American Institute of Chemical Engineers 1978, 24(6), pp 966–976.
21. Pitzer, K. S.; Mayorga, G. Thermodynamics of Electrolytes: II. Activity and Osmotic Coefficients for Strong Electrolytes with One or Both Ions Univalent. Journal of Physical Chemistry 1973, 77(19), pp 2300–2308.
22. Pitzer, K. S. Theory: Ion Interaction Approach. In Activity Coefficients in Electrolyte Solutions. CRC Press: Boca Raton, FL, 1979.
23. Pierrot, D.; Millero, F. J.; Roy, L. N.; Roy, R. N.; Doneski, A.; Niederschmidt, J. The Activity Coefficiencts of HCl in $HCl–Na_2SO_4$ Solutions from 0 to 50°C and Ionic Strengths up to 6. Journal of Solution Chemistry 1997, 26(1), pp 31–45.
24. Chen, C. C.; Evans, L. B. A local Composition Model for the Excess Gibbs Energy of Aqueous Electrolyte Systems. Journal of the American Institute of Chemical Engineers 1986, 32(3), pp 444–454.